Available online at www.sciencedirect.com

ScienceDirect

Procedia Engineering 213 (2018) 69–78

Procedia Engineering

www.elsevier.com/locate/procedia

7th International Conference on Fatigue Design, Fatigue Design 2017, 29-30 November 2017, Senlis, France

Predicting failure in additively manufactured parts using X-ray computed tomography and simulation

Johannes Fieres[a,*], Philipp Schumann[b], Christof Reinhart[a,*]

[a] *Volume Graphics GmbH, Speyerer Str. 4–6, 69115 Heidelberg, Germany, https://www.volumegraphics.com*
[b] *Concept Laser GmbH, An der Zeil 8, 96215 Lichtenfels, Germany, http://www.concept-laser.de*

Abstract

In casting, molding, or additive manufacturing processes, there are some typical issues that can change the geometry of a part and cause porosity or other defects. With the aid of X-ray computed tomography (CT), internal discontinuities and geometry deviations can be accurately detected and visualized. However, the question remains in how far a given defect affects mechanical failure. We aim at bridging this gap by structural mechanics simulations based on CT images. In this study, we describe a method to predict the tensile strength and the location of crack initiation from the simulated stress distributions on the basis of local stress concentrations. We validate the method for tensile rods and real-life aeronautic parts which were additively manufactured from an AlSi10Mg aluminum alloy. Thirty-six specimens were manufactured in total, where different porosity patterns were deliberately inserted. The specimens were CT-scanned in high resolution. Structural mechanics simulations were carried out on basis of the CT images. An immersed-boundary finite elements code is used. The generation of a conforming simulation mesh is not required, making the code suitable especially for complex geometries like porous objects. The same test specimens were subjected to destructive physical tensile tests. We show that there is a very good correlation between the predicted and measured tensile strengths, and that the location of the first crack occurrence can be forecasted accurately.

Peer-review under responsibility of the scientific committee of the 7th International Conference on Fatigue Design.

Keywords: computed tomography; CT; simulation; structural mechanics; immersed boundary methods; failure; tensile strength; porosity; additive manufacturing

1. Introduction

Structural parts almost inevitably differ from their ideal geometry due to the manufacturing process. In casting and injection moulding, gas or shrinkage pores are common kinds of defects. In additive manufacturing by sintering or melting, heat variations can cause imperfect bonding of the material granules.

Industrial X-ray computed tomography (CT) allows for the non-destructive detection and visualization of many kinds of superficial or internal defects. With today's CT scanners reaching spatial resolutions down to the micrometer scale, a CT image constitutes an accurate three dimensional digital representation of the scanned part. The spatial distribution and the morphological features of the porosity can thus be assessed in detail [1, 2]. However, the mere presence of porosity does not necessarily render a part unusable. In fact, even highly porous parts can still be good for a specific purpose. In order to minimize false rejections and

*Corresponding authors. {fieres,reinhart}@volumegraphics.com

1877-7058
Peer-review under responsibility of the scientific committee of the 7th International Conference on Fatigue Design.
10.1016/j.proeng.2018.02.008

thus production costs it is desirable to assess the "effect of the defect", i.e., to what degree a geometric defect affects the mechanical function. Work has been done to relate the detected porosity to fatigue behavior in aluminum castings [3] and laser-melted parts [4], sometimes combining the pore geometry with heuristic modeling of the pore physics [5, 6] or with analyzing stress concentrations at individual pores using finite element analysis [7].

In this study, we follow a more direct path by feeding the full three-dimensional digital model obtained from the CT scan into a mechanical stress simulation. Earlier work was going into this direction [3, 8]. However, real-life data can exhibit a rather complex geometry (e.g., ragged surfaces or fine-structured porosity), rendering the simulation task technically very challenging. In conventional finite element methods, the simulated domain must be tiled into a mesh of small volume primitives before a simulation can be conducted. This meshing step is crucial for the success of the simulation and can be challenging for complex geometries [3, 8], or even practically impossible [9], since contrary objectives are to be met. First, the mesh must be fine enough to capture all relevant geometric details. Second, the number of mesh cells must not be too large in order to keep the computational effort at a practical level. Third, the mesh cells must conform to certain shape criteria in order to assure the numerical stability of the simulation [10].

Recently, mesh-less and immersed-boundary finite element methods have been used to overcome the meshing problem [9, 11]. Such methods do not require the generation of a boundary-conforming mesh and are therefore suited for the simulation of arbitrarily complex domains as found in porous objects. The use of immersed-boundary methods with CT data was illustrated in [12] for a single pore embedded in the ideal component model. Entire highly-porous test specimens (castings) were simulated in [13], and results were compared to physical tests.

In the present work, 36 specimens with varying porosity were investigated by simulating their complete CT-scanned models on the pore scale using an immersed-boundary method. Simulated is a static load in the linear-elastic approximation followed by the analysis of the von Mises yield criterion. The simulations are matched against quasi-static physical tensile tests. The prediction of fatigue failure is commonly based on the analysis of linear statics with the aid of damage accumulation models (e.g., Wöhler curves). Thus, it makes sense to examine the static case for a proof of concept, even though more complex failure modes may be more relevant in many practical use cases.

In section 2, we describe the building, scanning, simulation, and physical testing of the specimens, and how we predict the tensile strengths from the simulation results on the basis of local stress maxima. In section 3, we present and discuss the actual results regarding the correlation of simulation and experiment and crack location. We conclude in section 4.

2. Methods

2.1. Test Specimens

In order to assess the effects of porosity, we need an ensemble of specimens with a varying degree of porosity. Modern additive manufacturing technologies allow to to build structures on scales as small as a tenth of a millimeter or less. This enables us to digitally design a 3d model of a specimen, to insert a precisely prescribed porosity structure, and to have it built exactly this way. Two 3d models were used as a basis: a) a standard tensile rod with 5mm diameter and 50mm length, and b) an aeronautic part. The aeronautic part is a bionically optimized structural bracket, originally approx. 150mm long, used in Airbus aeroplanes, built from Titanium using LaserCUSING®, a laser-melting additive manufacturing process by Concept Laser [14, 15]. The ideal 3d models were digitally deteriorated with different pore configurations. Six different pore configurations were created for each ideal model (Table 1). The test specimens were built by Concept Laser from an AlSi10Mg aluminum alloy, three copies per pore configuration, resulting in 18 rods and 18 aeronautic parts, i.e., 36 specimens in total. Five examples are shown in the photographs in Fig. 1. The aeronautic parts were built in half the original size, and none of the specimens was thermically post-treated, to save material and time.

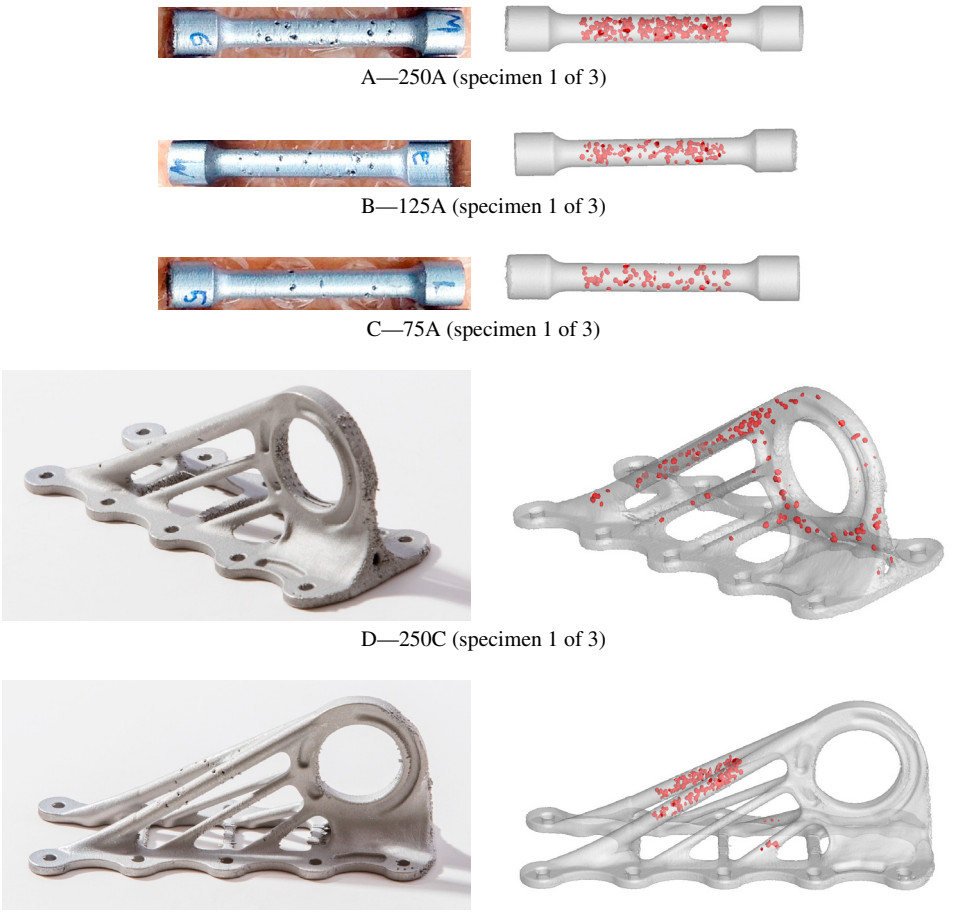

Fig. 1. Five out of 36 test specimens. A–C: Tension rods, D–E: Aeronautic parts. For each specimen: Left—photograph, before destructive test. Right—CT image data of same specimen, outer surface transparent, porosity highlighted in red.

2.2. Scanning and geometry reconstruction

CT scans were taken of the intact parts by the X-ray service provider *diondo* [16], with a resolution of 0.073 mm isotropic voxel size. The software VGSTUDIO MAX by Volume Graphics [17] was used to reconstruct the material surface from the CT scans, including all internal porosity, as depicted in Fig. 1. Unmelted metal powder remaining from the manufacturing process in the inner pores was clearly distinguishable in the CT images from solid metal by a darker gray level. The powder was considered as not absorbing any forces, and was treated as air in the subsequent simulations.

2.3. Simulation

Static structural mechanics simulations were performed based on the reconstructed surfaces from the CT scans. A linear-elastic isotropic material model was used with a Poisson's ratio of 0.3 which is a common choice for metals. The boundary conditions were set up as to mimic the physical tensile tests (Fig. 2). For the tensile rods, one end was fixed and the other end was subject to a unit pulling force. For the aeronautic parts, the ground plate was fixed at the screw holes, and a force was applied to the inner surface of the large bearing ring in a direction 29 degrees inclined from the ground plate.

The simulations were performed using the structural mechanics module of VGSTUDIO MAX by Volume Graphics [17] which is optimized for working with complex domains like porous material. As detailed in section 1, the mesh generation constitutes a major challenge in conventional simulators. VGSTUDIO

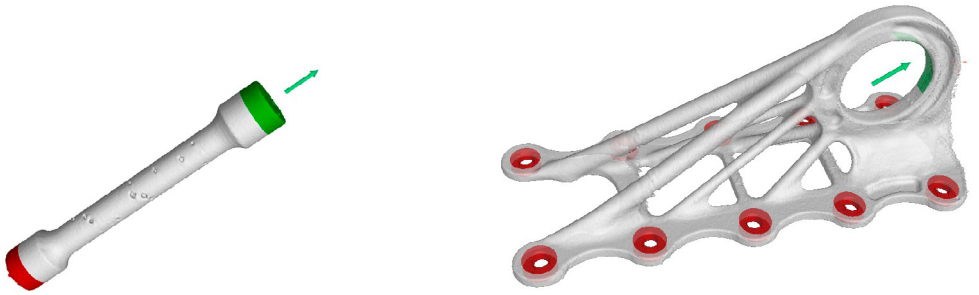

Fig. 2. Setup of simulation boundary conditions for the tensile rods and the aeronautic parts. Red—fixed surface; green—surface subject to traction; green arrow—force direction.

MAX does not require a polygon mesh at any point in the processing tool-chain. The reconstructed surface of the CT-scanned part is represented in an implicit manner directly sourcing the image data. The solver is based on an immersed boundary method and as such does not require a geometry-conforming mesh. It works directly on the implicitly represented surface.

2.4. Physical Tensile Tests

Quasi-static tensile tests were conducted on all specimens. The specimens were elongated in uni-axial stress until complete rupture (tensile rods) or until the occurrence of the first crack (aeronautic parts). The bearing force was measured as a function of elongation and recorded into a stress-strain curve. The tensile rods were threaded at their ends and fixed in a standard specimen holder. The aeronautic parts were screwed with their ground plate to a massive base while a pulling force was applied with a bolt fitted through the bearing ring (Fig. 3). The base was tilted resulting in a force direction of 29 degrees from the ground plate (equal to the inclination of the bar structures).

Since we are interested in the occurrence of the first crack, the tests of the aeronautic parts were stopped manually as soon as the first cracks were visible. Due to the human reaction time and the lag of the machine control, many specimens were completely ruptured nevertheless.

2.5. Data Analysis

2.5.1. Prediction of tensile strength and crack location

The static structural mechanical simulations provide the local stress tensor at all points within the undeformed specimen. Further analysis is necessary in order to deduce predictions about the real failure behavior. Our aim is to predict both the location of the first crack and the tensile force necessary to initiate the first crack. The analysis is based on the Mises stress σ_M, a scalar quantity, which we calculate at any point in the object from the simulated stress tensor. The Mises stress is a commonly used predictor of yielding in metals. When it exceeds a critical value known as the material's *yield strength*, the material can be assumed to leave the elastic regime and start yielding.

Table 1. Pore configurations used to build the test specimens.

a) Tensile rod

Label	Comment
75A	75 randomly distributed ellipsoid pores
75B	as above, different random configuration
125A	125 randomly distributed ellipsoid pores
125B	as above, different random configuration
250A	250 randomly distributed ellipsoid pores
250B	as above, different random configuration

b) Aeronautic part

Label	Comment
250C	250 randomly distributed ellipsoid pores
250D	as above, different random configuration
Base200	200 rand. distr. pores in the base area only
Bars200	200 rand. distr. pores in the bars area only
Notch	A severe notch in the base area
Plain	No defects

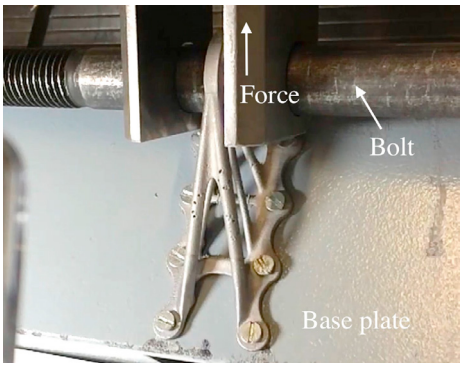

Fig. 3. Experimental setup for physical stress test of the aeronautic part. The part is screwed to an inclined massive metal base plate. The force is applied in vertical direction with a bolt passing through the bearing ring.

All simulations were performed with a unit total applied force. In the tensile tests the force increases monotonically, up to the first damage. Given that the Mises stress scales proportionally to the applied force (which is assumed in the linear-response approximation of the material and for small enough deformations) the yield strength is reached first at the location where the Mises stress at unit force takes on its global maximum. This is where we predict the first crack to initiate:

$$\mathbf{x}_{\text{crack}} = \operatorname*{argmax}_{\mathbf{x}\in\mathcal{V}} \sigma_M(\mathbf{x}), \tag{1}$$

where $\mathcal{V}$ is the volume domain of the simulated part. Further, when comparing different specimens, the total force necessary to initiate the first crack, F_{crack}, is predicted to be proportional to the inverse of the maximum Mises stress at unit force:

$$F_{\text{crack}} \propto \frac{1}{\max_{\mathbf{x}\in\mathcal{V}} \sigma_M(\mathbf{x})}. \tag{2}$$

In practical simulations, we often find a few local stress maxima with stress values only slightly less than the global stress maximum. In the following we will denote local stress maxima by the more intuitive term *hot-spots*. The used software automatically detects all hot-spots and sorts them by their Mises stress. We denote the Mises stress at the first hot-spot by HS_1. It is equal to the global Mises stress maximum. The subsequent hot-spots HS_2, HS_3, etc., are the next largest local maxima in descending order. Due to various uncertainties in modeling, imaging, surface reconstruction, and simulation, the first crack seen in the physical experiment does not always happen at HS_1, but it will happen at any of the first few hot-spots. To level out the uncertainties to some amount, we take the average of the largest N hot-spots

$$\langle \text{HS} \rangle_N = \sum_{n=1}^{N} \text{HS}_n, \tag{3}$$

and use this to predict the tensile strength instead of equation (2):

$$F_{\text{crack}} \propto \frac{1}{\langle \text{HS} \rangle_N}. \tag{4}$$

We choose $N = 3$ in this study. This choice does not seem to be very critical. We tested $N = 1 \ldots 4$, not changing the reported results qualitatively.

In this study, no attempt is made to predict the proportionality factor in equations (2) or (4). One may naively assume it could be determined by substituting the (known) yield strength of the material in the equations. In practice, there exist various systematic limitations in both the accuracy of imaging and analysis, and the modeling of the crack physics. For the former, cracks will actually initiate at small tips induced by microscopic surface roughness. Even a high-resolution CT scan cannot resolve all relevant

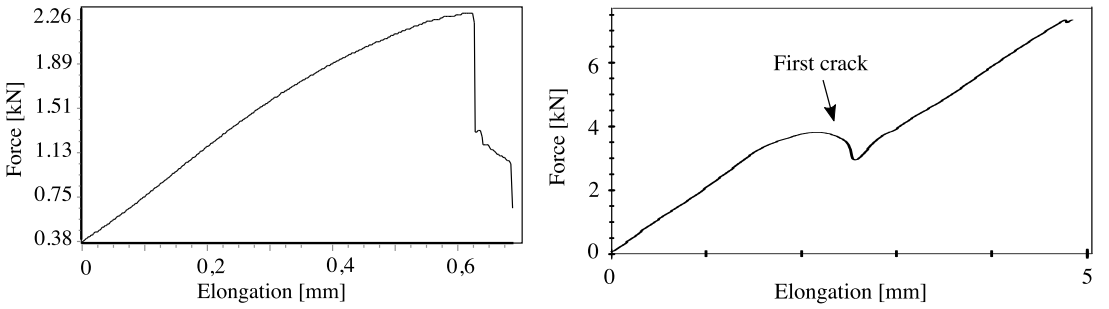

Fig. 4. Examples of physically measured stress-strain curves. Top—Tensile rod 250A (specimen 1 of 3); bottom—Aeronautic part 250C (specimen 1 of 3). The sudden force drop in the right diagram indicates the occurrence of the first crack.

micro-structures. As well the numerical simulation is done with finite spatial resolution. For the latter, the employed linear elastic model does not capture all effects happening at a sharp tip, just before a macroscopic crack occurs. In reality, ductile effects are believed to alleviate high stress concentrations to a certain amount. In this sense, the described method is a heuristic one.

2.5.2. Analysis of Tensile Tests

The tensile tests result in stress-strain curves. Examples are depicted in Fig. 4. The maximum point in a stress-strain curve indicates the ultimate tensile stress, i.e., the point of complete rupture where the specimen cannot bear any force anymore. However, the method described in the previous section is designed to predict the occurrence of the first crack. For the tensile rods, this happens to coincide with the ultimate tensile stress, probably due to an avalanche effect. For the aeronautic parts, due to their more complex geometry, the occurrence of the first crack does not always cause immediate total destruction. Instead, the stress at the first crack is relieved and redistributed to other structural elements, allowing for a further increase in force. These events are visible in the stress-strain curve as sudden drops in stress followed by a recovery (see indicator in Fig. 4, right diagram). For the aeronautic parts, the maximum in the stress-strain curve before the first sudden drop was determined and identified with F_{crack} in equation (4).

3. Results and Discussion

3.1. Tensile strength

The physically measured fracture force is plotted versus the prediction in Fig. 5. The numeric cross-correlation is 0.96 for the tensile rods and 0.78 for the aeronautic parts.

Some interesting observations shall be noted:

The rod configurations 75(A,B) and 125(A,B) differ in the number of pores (75 vs. 125 pores). Looking at the porosity only, one would assume that the 75(A,B) configurations are generally more stable than 125(A,B). Fig. 5a, however, reveals that this is not the case. First, 125B is actually approximately as stable as 75B, both in physical tests and in the simulations. Second, 125A is even more stable than 75B in the physical tests. This is in accordance with the simulations when regarding the average of each three specimens.

With the aeronautic parts, the variations in stability are significant even within specimens of the same pore configuration. The variations due to the manufacturing process seem to be relevant and their effect on stability can be predicted by the proposed method.

Among the aeronautic parts, the Notch configuration stands out as the red crosses in Fig. 5b do not seem to fit the least-squares line defined by the other data points only (dotted line in Fig. 5b). The numeric correlation between experiment and simulation raises from 0.78 to 0.86 when ignoring the Notch configuration. It is a notable coincidence that the Notch configuration represents a different type of porosity. All other configurations were generated by inserting ellipsoid voids into the part. The Notch configuration was created by digitally etching a severe groove into the part using 3d image manipulating software (see the horizontal opening in Fig. 6, 3rd row, right image). The observed data suggests that the proposed method

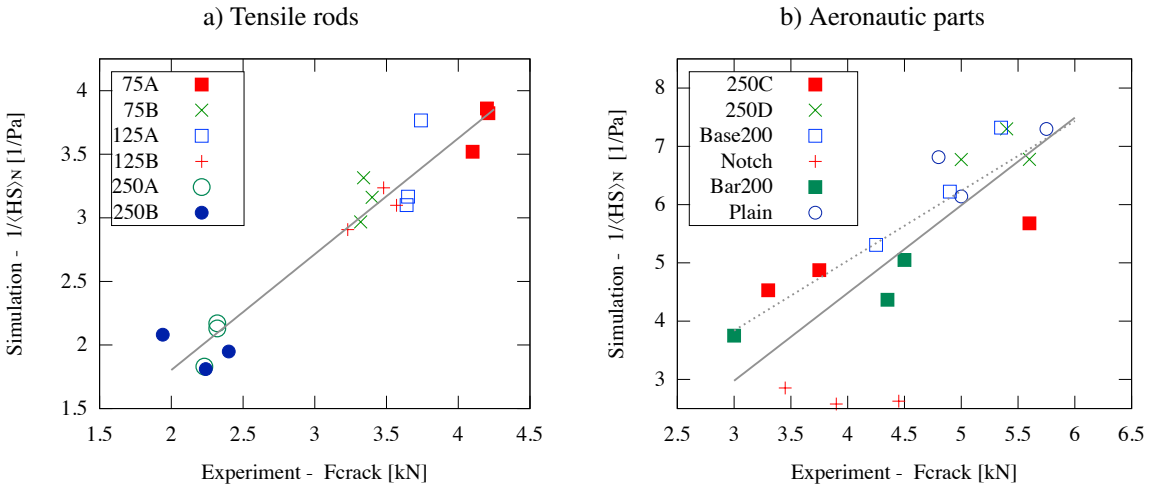

Fig. 5. Measured force at first crack (F_{crack}) versus prediction from simulation ($1/\langle \text{HS} \rangle_N$). Each data point represents one tested specimen. Left—tensile rods; right—aeronautic parts. The straight line is a least-squares fit to the data. Dotted line: see text in section 3.1.

works best when comparing specimens with a somehow similar defect morphology. This is in accordance with the limitations of the method stated at the end of section 2.5.1.

3.2. Crack location

As detailed in section 2.5.1, the hot-spots (local maxima) in the simulated stress distribution, HS_i, can be treated as a list of predicted crack locations, sorted by likelihood. The likelihood decreases with increasing hot-spot index i. HS_1 is the most likely guess, HS_2 is the second likely guess, and so on. For the aeronautic parts, the correlation of the hot-spot locations with the physically observed crack locations was investigated in detail. It turns out that for 12 out of the 18 specimens, a crack did actually occur at the first or second most-likely predicted location. For 3 specimens, cracks did occur within the top-ten most-likely predicted locations. Only for the remaining 3 specimens (incidentally, all 250D specimens), there was no coincidence between any predicted and real crack location. Fig. 6 shows the simulated versus predicted crack locations for five selected specimens.

All specimens contained artificial defects except for the three specimens labeled Plain. The Plain specimens were designed without defects. It turns out that even these specimens contain some amount of porosity due to process variations in manufacturing. We note that the crack locations in these samples were predicted fairly well, as a real crack occurred at the predicted hot-spots HS_2, HS_8, and HS_1 for the three specimens 1, 2, and 3, respectively. Fig. 7 shows the stress concentration around a pore spontaneously occurring during manufacturing. This stress concentration was the most likely predicted crack location in the simulation and the location of fracture in the tensile test (cf., Fig. 6, 6th row).

4. Conclusions and Outlook

We described a method to predict the location of the first crack and the tensile force necessary to initiate the first crack for porous aluminum parts. The method is based on a high-resolution CT scan of a part, a subsequent static structural mechanics simulation of the scanned model, and, finally, the analysis of local maxima of the simulated stress distribution.

We showed in validating experiments that the predictions are very accurate, despite of systematic limitations in the spatial resolution of the scan and the simulation, and the simplified modeling of the crack physics. In this sense, the method shows to be robust.

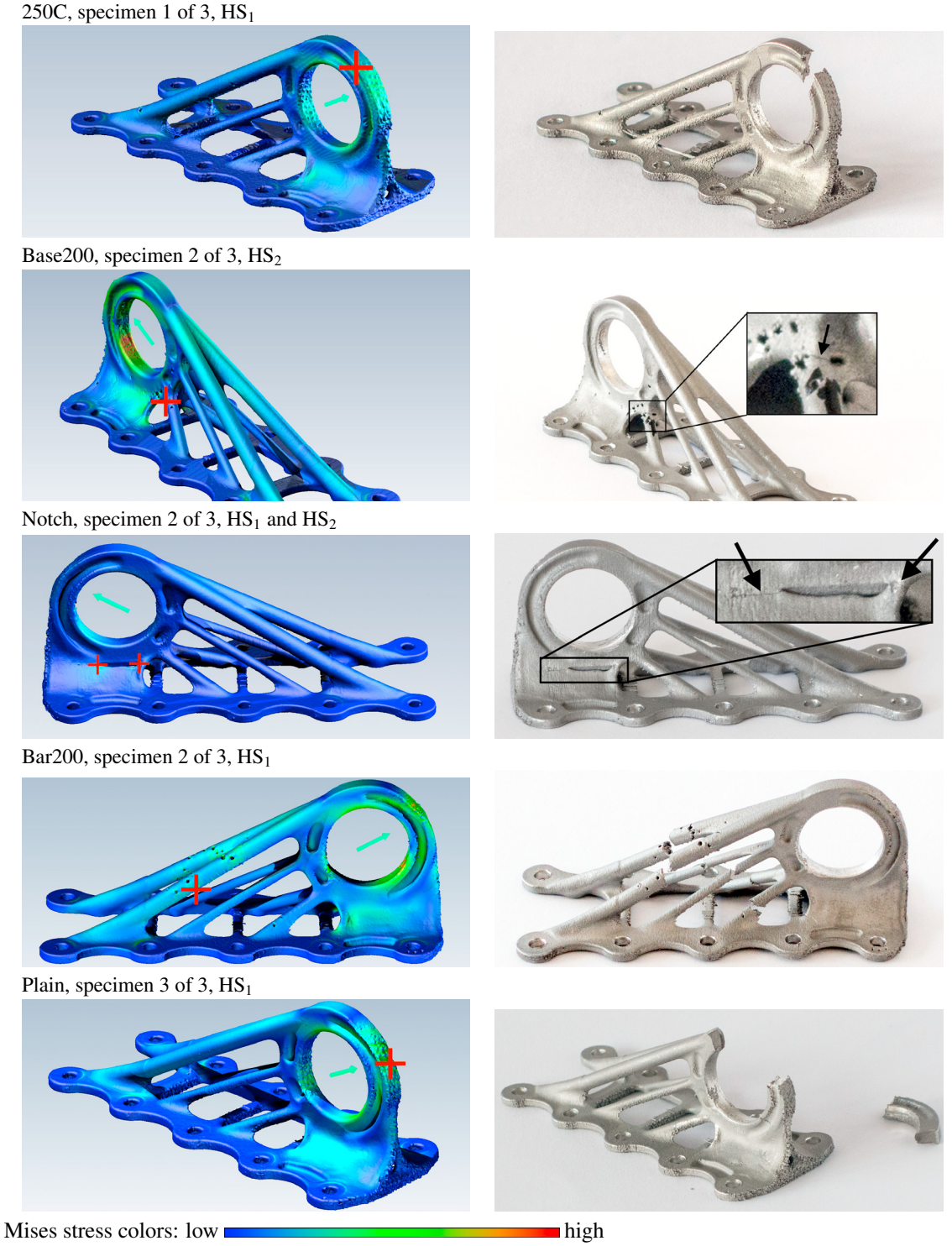

Fig. 6. Predicted versus real locations of fracture for five examples. Left column—Digital reconstruction from CT-scan of intact part. Simulated Mises stress shown as color overlay. Predicted fracture location indicated by red cross. Rows 1, 4, and 5: cross=global Mises maximum (HS_1); row 2: cross=second-largest local Mises maximum (HS_2); row 3: crosses=global and second-largest Mises maxima (HS_1, HS_2). Right column—photographs of parts after tensile tests.

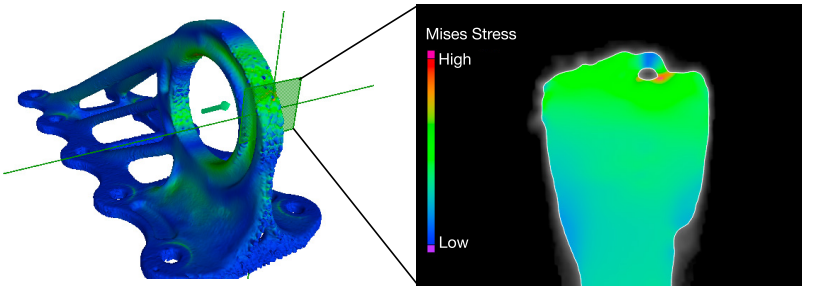

Fig. 7. CT scan with color overlay of Mises stress for a specimen without artificial defects (configuration Plain, specimen 3 of 3). This specimen contains only porosity spontaneously occurring in the manufacturing process. The stress concentration at the pore shown in the slice section was correctly predicted to be a crack location.

Only static loading was considered here even though fatigue due to dynamic loading is of greater interest in many realistic scenarios. Since fatigue is commonly modelled on the basis of quasi-static stress distributions with the aid of cumulative damage models we assume that the good correlation between simulation and experiment will also hold for fatigue due to time dependent loading.

The experiments were conducted with additively manufactured aluminum parts where porosity was deliberately built in. The analysis of variations among specimens within the same pore configuration suggest that the effects of the non-intended porosity occurring in the laser-melting additive manufacturing process can as well be predicted. Whether this method also works for typical porosity occurring in casting and molding remains to be studied. The cast specimens examined in [13] were too similar in their ultimate tensile strength to see a significant correlation with the simulations, yet a moderate correlation was observed. The similarity of tensile strength in that case was due to the pores being in the same location (centre) of all studied samples. Yet unpublished data from eight die-cast tensile rods, however, suggest that the method can be applied here without changes.

Acknowledgments

We thank Airbus Emerging Technologies & Concepts for the permission to use the bionically optimized bracket model. We thank diondo X-ray Systems and Services, Hattingen, Germany, for performing the CT scanning. We would also like to thank Henry Weber at Volume Graphics for creating the renderings and photographs in Figs. 3 and 6, and Joel Micah Miller for creating the photographs D and E in Fig. 1.

References

[1] E. Maire, P. J. Withers, Quantitative X-ray tomography, International Materials Reviews, 59(1) (2014) 1–43.
[2] A. du Plessis, P. Rossouw, X-ray computed tomography of a titanium aerospace investment casting, Case Studies in Nondestructive Testing and Evaluation 3 (1025) 21–26.
[3] Q. Wan, H. Zhao, and C. Zou, Effect of micro-porosities on fatigue behavior in aluminum die castings by 3D X-ray tomography inspection, ISIJ international 54(3) (2014) 511–515.
[4] S. Siddique, M. Imran, M. Rauer, M. Kaloudis, E. Wycisk, C. Emmelmann, F. Walther, Computed tomography for characterization of fatigue performance of selective laser melted parts, Materials & Design 83 (2015) 661–669.
[5] J.P. Weiler, J.T. Wood, R.J. Klassen, E. Maire, R. Berkmortelc, G. Wangc, Relationship between internal porosity and fracture strength of die-cast magnesium AM60B alloy, Mater. Sci. Eng. A 395 (2005) 315–322.
[6] C.H. Cceres, B.I. Selling, Casting defects and the tensile properties of an Al—Si—Mg alloy, Mater. Sci. Eng. A 220 (1996) 109–116.
[7] G. Nicoletto, R. Konen, S. Fintova, Characterization of microshrinkage casting defects of AlSi alloys by X-ray computed tomography and metallography, Intern. J. of Fatigue 41 (2012) 39–46.
[8] E. Maire, A. Fazekas, L. Salvo, R. Dendievel, S. Youssef, P. Cloetens, J.M. Letang, X-ray tomography applied to the characterization of cellular materials. Related finite element modeling problems, Composites sci. and technology 63(16) (2003) 2431–2443.
[9] V.P. Nguyen, T. Rabczuk, S. Bordas, M. Duflot, Meshless methods: a review and computer implementation aspects, Mathematics and computers in simulation 79.3 (2008): 763-813.
[10] J.R. Shewchuk, What Is a Good Linear Finite Element? Interpolation, Conditioning, Anisotropy, and Quality Measures (Preprint), University of California at Berkeley 73 (2002).

[11] D. Schillinger, M. Ruess, The Finite Cell Method: A Review in the Context of Higher-Order Structural Analysis of CAD and Image-Based Geometric Models, Arch. Comp. Meth. Engin. 22(3) (2015) 391–455.
[12] S. Duczek, H. Berger, U. Gabbert, The Finite Pore Method A new approach to evaluate gas pores in cast parts by combining computed tomography and the finite cell method, Int. J. Cast Metals Research 28(4) (2015) 221–228.
[13] A. du Plessis, I. Yadroitsava, S.G. le Roux, I. Yadroitsev, J. Fieres, C. Reinhart, P. Rossouw, Prediction of mechanical performance of Ti6Al4V cast alloy based on microCT-based load simulation, Journal of Alloys and Compounds 724 (2017) 267–274.
[14] Airbus, Inc., Printing the future: Airbus expands its applications of the revolutionary additive layer manufacturing process, web article (2014), http://www.airbus.com/presscentre/pressreleases/press-release-detail/detail/printing-the-future-airbus-expands-its-applications-of-the-revolutionary-additive-layer-manufacturi/ (loaded May 17 2017).
[15] Concept Laser GmbH, Lichtenfels, Germany, https://www.concept-laser.de (loaded May 17 2017).
[16] diondo GmbH, Hattingen, Germany, http://http://www.diondo.com
[17] Volume Graphics GmbH, Heidelberg, Germany, https://www.volumegraphics.com (loaded May 17 2017).